Solid Freeform Fabrication 2017: Proceedings of the 28th Annual International Solid Freeform Fabrication Symposium – An Additive Manufacturing Conference
Reviewed Paper

MICROSTRUCTURE AND MECHANICAL BEHAVIOR OF AlCoCuFeNi HIGH-ENTROPY ALLOY FABRICATED BY SELECTIVE LASER MELTING

M.N. Zhang, X. L. Zhou*, W. Z. Zhu, J. H. Li

State Key Laboratory for Advance Metals and Materials, University of Science and Technology, Beijing 10083, People's Republic of China
*Corresponding author at: State Key Laboratory for Advance Metals and Materials, University of Science and Technology, Beijing 10083, People's Republic of China. Tel: 8682375385.
Email addresses: coldspray@163.com

Abstract

Additive manufacturing (AM) technique, such as selective laser melting (SLM) is a modern method for materials fabrication and formation. In this study, AlCoCuFeNi HEA parts are fabricated by SLM using pre-alloyed powders prepared by atomization process. The effect of processing parameters on microstructures, microhardness and compression property of SLM-fabricated HEA parts are systematically investigated. Results show that input laser energy density involved in laser power and scan speed plays a significant role in the densification behavior. A near-full 99.03% density is achieved as an energy density of 102.5 J/mm^3. The alloys consist of simple body-centred cubic (BCC) structure and exhibit the highest microhardness up to 541.17 $HV_{0.2}$ and compressive strength of 1621.1 MPa due to the BCC solid solution strengthening. The study reveals that SLM is advantageous to produce the high-entropy alloy with high density, good mechanical properties and even complicated shapes.

Keywords

Selective laser melting (SLM); High-entropy alloy; Densification; Microstructure; Microhardness

Introduction

High-entropy alloys (HEAs) with multi-principal elements have experienced extensive research and attract enormous attention over the past decade [1]. It is typically composed of at least five major constituents with each elemental concentration between 5 and 35 at.%, which breaks through the design strategy of traditional alloys based on one or two principle elements [2]. Due to its high mixing entropy, the simple solid solution structure with multi-elements is easier formed in the HEAs during solidification instead of intermetallic compounds, such as body-centered cubic (BCC), face-centered cubic (FCC) and/or hexagonal close-packed (HCP) structures [3-4]. HEAs have been reported to possess great potential for engineering applications attributed to their many unique properties, such as high hardness, good mechanical strength and ductility, high wear and corrosion resistance and excellent thermal stability [5-8].

High-entropy alloys are usually prepared by arc melting technology or casting methods [9-10]. However, these conventional processing techniques are limited to widespread use of HEAs in highly demanding applications, such as component segregation due to sluggish cooling rate and high costs in the preparation of bulk materials. In addition, the sizes and shapes of bulk ingots prepared using these techniques are limited. To solve these problems, additive manufacturing (AM) such as selective laser melting (SLM), laser engineered net shaping (LENS) and electron beam melting (EBM) technologies, called three-dimensional (3-D) printing, have received much attention in the recent years [11-12]. This technique can automatically fabricate multifunctional parts in a layer-by-layer manner directly from three-dimensional computer-aided design (CAD) model. Compared to traditional subtractive manufacturing methods, AM can create complex shapes and controlled porosity in a shorter time and with lower cost.

Up to date, a large amount of efforts have been focused on the fabrication of metals and alloys parts using AM and it is verified the feasibility of building a metal part from a range of powders, including stainless steel, titanium alloys and nickel superalloys [13-16]. Moreover, AM study of high-entropy alloys has gathered great deal of attention and is still developing. For instance, I. Kunce et al. [17] successfully fabricated thin-walled samples of the AlCoCrFeNi high-entropy alloy using the laser engineered net shaping (LENS) method, which demonstrated that the laser scan rate had a significant effect on the microstructure, and increasing the cooling rate reduced the average grain size of the LENS-produced alloy. Jithin et al. [18] also studied the bulk AlCoCrFeNi high-entropy alloy manufactured by direct laser fabrication (DLF) from simple elemental powder blends. It was concluded that microstructure and mechanical properties of the direct laser sintered samples were very similar to those produced by arc melting, indicating DLF was a successful technique to fabricate bulk high-entropy alloys. And recently, Hiroshi et al. [19] had carried out a comprehensive study of fabricating equiatomic AlCoCrFeNi HEA prepared via selective electron beam melting (SEBM). The SEBM alloy possessed fine modulated structure of the B2/BCC phases and exhibited much higher plastic deformability than the cast specimen, without significant loss of strength. In addition, Yevgeni et al. [20] reported that FeCoCrNi high-entropy alloy successfully fabricated using SLM and the part with fine microstructure and enhanced mechanical properties is obtained. It showed that SLM technology was a promising method to fabricate the HEAs and showed great potential. In this study, equiatomic AlCoCuFeNi high-entropy alloy is fabricated by SLM using pre-alloyed powders. The effect of processing parameters on phases, microstructure, density and mechanical property of SLM-fabricated HEA parts is systematically studied and discussed in detail.

2. Experimental

The starting material used in this study is gas atomized AlCoCuFeNi high-entropy alloy powder. The main chemical composition of the powder is given in Table 1. The HEA powders show a spherical morphology (Fig.1 (a)) in the size range of 15-53 μm with an average of 30 μm (determined by Malvern laser particle size analyzer). The particle size distribution is displayed in Fig. 1(b).

Table 1: Chemical composition of the employed powder determined by EDX analysis

Powder material	Al	Co	Cu	Fe	Ni
HEA	20.43	20.43	19.19	22.39	17.55

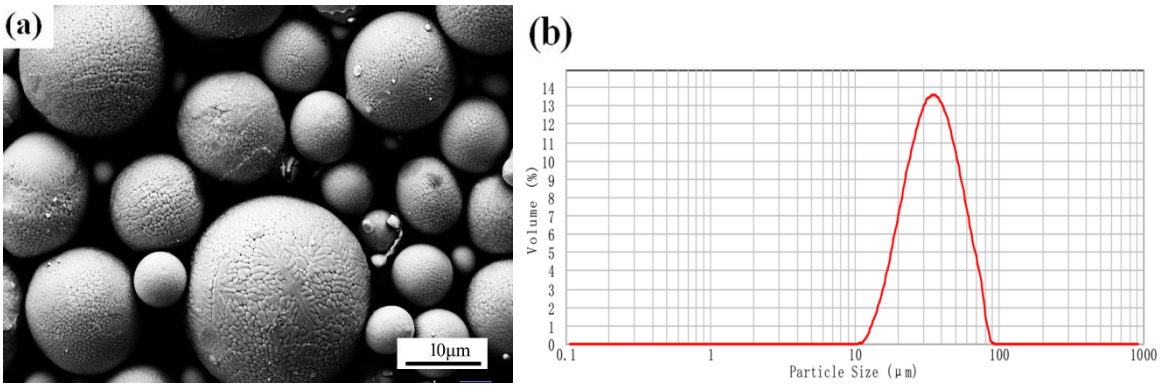

Fig. 1 AlCoCuFeNi high-entropy alloy powder: (a) particles morphology, (b) powder particles size distribution.

The experiments are carried out on a commercial SLM 250 (YZSLM-250) machine equipped with a 500 W fiber laser that has a wavelength of 1.07 μm. The diameter of the focused laser spot size is about 30 μm. The maximum laser power and scanning speed are 500 W and 5000 mm/s respectively. The layer thickness is constant at 30 μm and the hatch spacing is always 40 μm. All SLM parts are produced in a closed environment filled with argon as a protective gas. The oxygen content in the build chamber is controlled to < 0.1% and to

prevent the oxidation of iron during the fabrication process. Based on a series of preliminary experiments, in this study, the parameters used for preparing the samples are shown in Table 2. During fabrication by SLM, an alternating x/y raster scan strategy is used to build each part. The direction of scanning is rotated at 90° between consecutive layers. Also, the laser energy density E (J/mm^3) is used to appraise the density of the parts and to optimize the parameters, which is defined as the energy supplied by laser beam in unit volume as shown in Eq.(1) [21] :

$$E = \frac{P}{vht} \quad (1)$$

Where P is the laser power (W), v is the scanning speed (mm/s), h is the hatching space (mm), and t is the layer thickness (mm).

Table 2: Parameter range used for SLM of HEA

Samples	Laser powder [W]	Scan speed [mm/s]	Energy density [J/mm^3]
S1	185	1000	92.5
S2	195	1000	97.5
S3	205	1000	102.5
S4	195	900	108.3
S5	195	800	121.8

For microstructure analysis, samples are prepared using standard techniques and chemically etched at room temperature, by a solvent composed of 97 ml and 3 ml HNO_3 (every 100 ml solution). The microstructure is determined using the optical microscopy (OM, Axio Imager) and the scanning electron microscopy (SEM, ZEISS SUPRA 55) operated at back-scatter electron (BSE) mode. The chemical compositions of different selected micro-areas are analyzed by SEM energy dispersive spectrometry (EDS), and phase identification is characterized by PHILIPS APD-10 X-ray diffraction (XRD) with Cu target whose characteristic wavelength λ (Kα1) = 1.54056 Å. The working voltage and current are 40 kV and 40 mA, respectively. The scan range is from 10° to 90°, and the scanning rate is 2°/min. The density of the parts is measured bythe Archimedes method. The parts are weighed in air and in ethanol to determine the density. In this work, the relative density is depicted as a percentage of the material's theoretical density of 2.68 g cm^{-3}. The micro-hardness tests are carried out on the as polished surface using a Vickers hardness tester (HXD-1000TM) by applying 200 g load for a duration time of 10 s. Each sample is measured at least seven sets of data, take the average hardness as the final outcome.

3. Results and Discussion

3.1 Relative density

The density of SLM-processed samples is measured by the Archimedes method and image analysis method. The effect of laser energy density on the relative density is shown in Fig. 2 and the surface morphologies of corresponding samples processed using various parameters is illustrated in Figs. 3. The density of the samples increases with the increasing the energy density up to 102.5 J/mm^3, at which point the density of samples is greater than 99%, i.e., nearly full density, which can be seen from Fig. 2. When laser energy density is less than 102.5 J/mm^3 (samples S1 and S2), more irregular-shaped cracks or pores can be observed in the surface morphology as shown in Figs. 3(a) and (b). This is because that the powder could be incompletely molten due to lower energy put, that result in the occurrence of balling phenomena and unmelted particles formation. Therefore, the balling and dross may cause the development of pores and dross that even detriment extremely the surface integrity and densification of the parts, which can be confirmed by Fig. 2. On increasing the energy density up to 102.5 J/mm^3, a number of pore defects are eliminated and only very small spherical

pores are sporadically observed in the sample S3 as depicted in Fig. 3 (c) and (d). This is because the relatively enhance laser energy density resulted from increasing the laser power or decreasing the scanning speed lead to a higher temperature of the melting pool. It is evident that, during the laser scanning, higher laser power could provide sufficient heating energy to melt the powders, and the slower scanning speed could ensure a longer time to melt all powders layer completely. Thus the appropriate energy density is able to make a stable molten pool at optimized parameters combinations of laser power and laser scanning speed. Moreover, the relative density becomes steady and then slightly drops with the energy density increases as seen from Fig. 2. It is due to the increment of energy input lead to an increase in melt pool size resulted from melting the adjacent powder, and then making not enough powders for the following scanning and melting. Consequently, more metallurgical pores formed in the part when the excessive energy input as shown in Fig 3 (e).

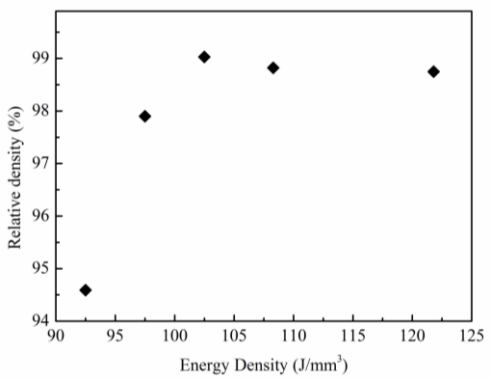

Fig. 2 Relative density of SLM processed samples at various energy densities.

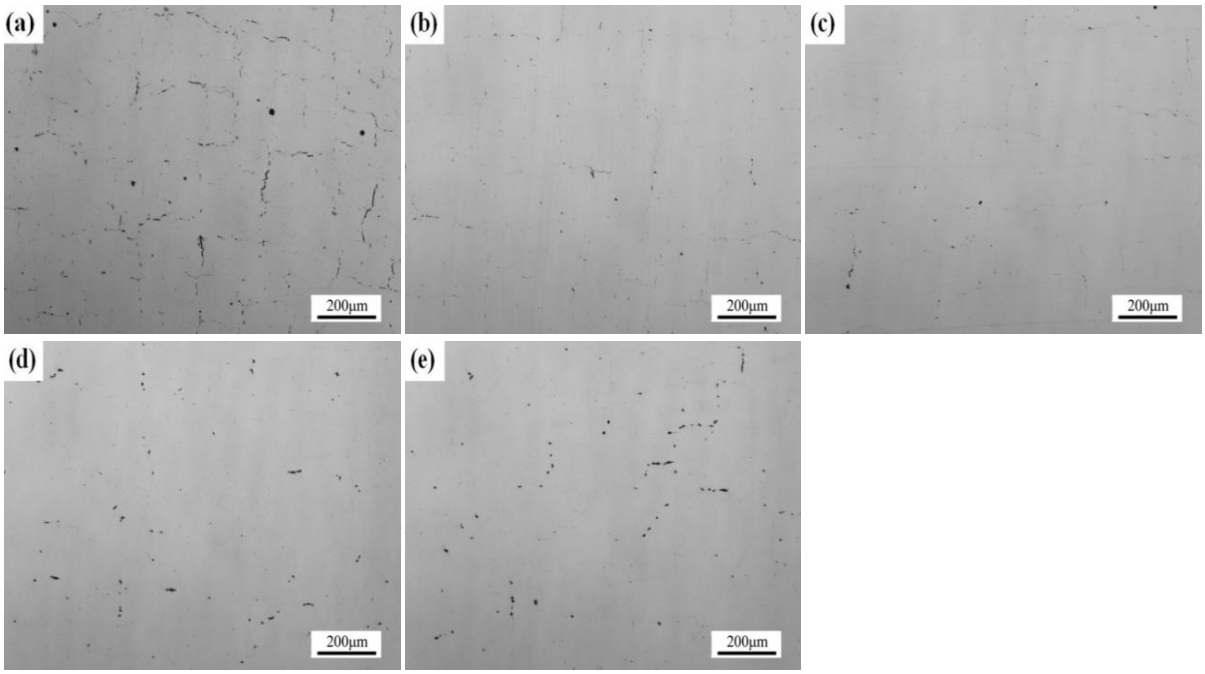

Fig. 3 Optical micrograph images of SLM processed samples.

3.2 Phase analysis and microstructure characterization

X-ray diffraction (XRD) patterns of AlCoCuFeNi high-entropy alloys manufactured by SLM are shown in Fig. 4(a). All diffraction peaks are identified as a simple ordered body-centred cubic (BCC) crystal structure. On the basis of Gibbs phase rule, $F = C - P + 1$ (Here F is a degree of freedom, C is the number of components, and P is the number of phases), the number of equilibrium phases in a C component system at constant pressure is $P = C + 1$, while the $P > C + 1$ holds true for the non-equilibrium solidification phase number. However, in

this research, the phase number of AlCoCuFeNi HEA is much less than the maximum equilibrium number of 6 given by the Gibbs phase rule. The formation of single BCC solid solution phase is attributed to the high mixing entropy effect, which is common in the case of equiatomic multicomponent alloys. The mixing entropy of an alloy with 5 elements in equal-molar ratio is 13.37 J/kmol. The high mixing entropy from multi-principal elements thus can effectively increase the confusion extent in the alloys and favor the formation of a solid solution. Figs. 4(b)-(d) show the backscattered electron micrograph (SEM) and EDS compositional analysis of the SLM-processed S3 sample. SEM images of the high-entropy alloy further confirm the single-phase BCC structure, and the additive alloying elements are distributed in the multi-element BCC solid solution. The EDS results clearly demonstrate that all elements are uniformly distributed with no visible segregation. This is due to the sluggish diffusion of the alloying elements, which is one of the main features of high-entropy alloys. Fig. 4(d) shows the optical micrograph of the SLM-processed sample S3. The sample is polished and etched by the mixture of nitric acid 3 ml and alcohol 97 ml. It can be seen that the cross-section view of the melt pool produced by different layers is visible, which indicates that complete melting of the powder occurred. The interwoven laser scan tracks and hatching between two neighbor layers demonstrate the similar scan strategy in horizontal and longitudinal direction between alternating layers.

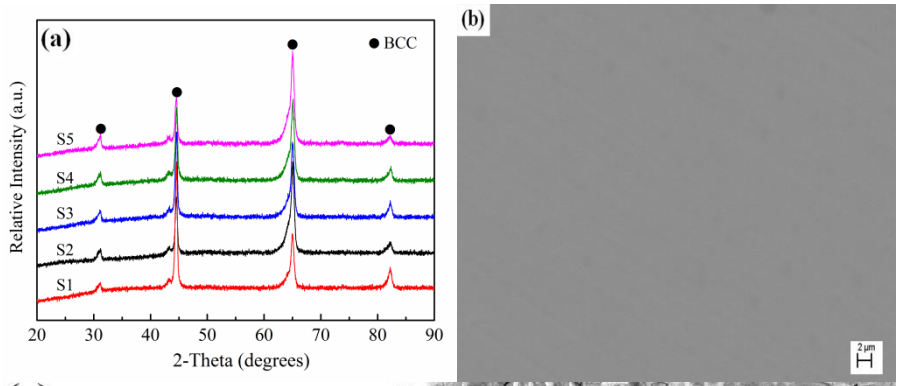

S3	At.%	Wt.%
Al	19.30	9.82
Cu	20.01	23.98
Co	20.31	22.57
Fe	20.04	21.11
Ni	20.34	22.53

Fig. 4 XRD analysis and microstrucuture of the SLM-processed samples.

3.3 Mechanical properties

Fig. 5 shows the variation of microhardness for all SLM-processed high-entropy alloy samples. As it can be seen, the SLM-processed AlCoCuFeNi HEA possesses a relatively high hardness and the maximum microhardness value reaches up to 541.17 $HV_{0.2}$ for sample S3, which is greater than that of processed by conventional arc-melting manufacturing techniques [22]. This enhancement of hardness is ascribed to the solid solution strengthening of the BCC solid solution phases in the alloys as shown in Fig. 4. Moreover, the microhardness of SLM-processed parts exhibits an obvious increase from sample S1 to sample S3, and then for the sample S4 and sample S5 alloys, the hardness values undergoes slight decrease as the increment of laser energy input. It is therefore apparent that the hardness changes synchronously with the increment of laser energy input and there is a strong correlation between hardness and density. The microhardness is enhanced by

improvement of densification. The decrease in the micohardness can be attributed to the present of defects in the samples with reduced relative density.

Compressive stress-strain curve of the SLM-processed high entropy alloys is shown in Fig. 6 (a) at room temperature, and Fig. 6 (b) displays the corresponding compressive feature image. The compressive strength of the alloys improves significantly as the energy density is increased, and the sample S3 shows the highest compressive fracture strength, which is as high as about 1621.1 MPa. This high compressive strength may be mainly due to the BCC solid solution from multi elements. The difference in components atomic radius results in larger lattice distortion, and thus enhances the solid-solution strengthening effect. For the sample S1 and S2 alloys, the compressive strength decrease with a reduced relative density. In the compression test, the pores or unmelted powder particles in the alloys may lead to stress concentration, which is harmful to the strength. Cleavage steps are observed on the fracture surface as shown in Fig. 6(b), we can see that, the type of fracture is brittle cleavage. The rough facts in the fracture surface indicate the poor ductility.

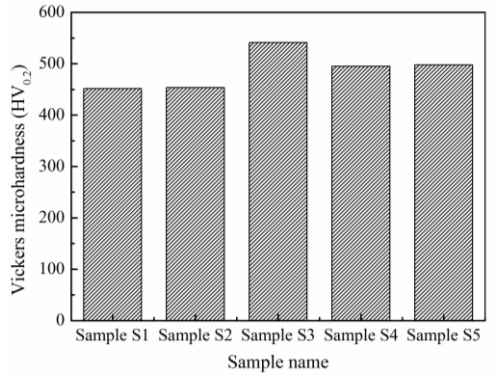

Fig. 5 Micro hardness variation of the SLM-processed HEA samples.

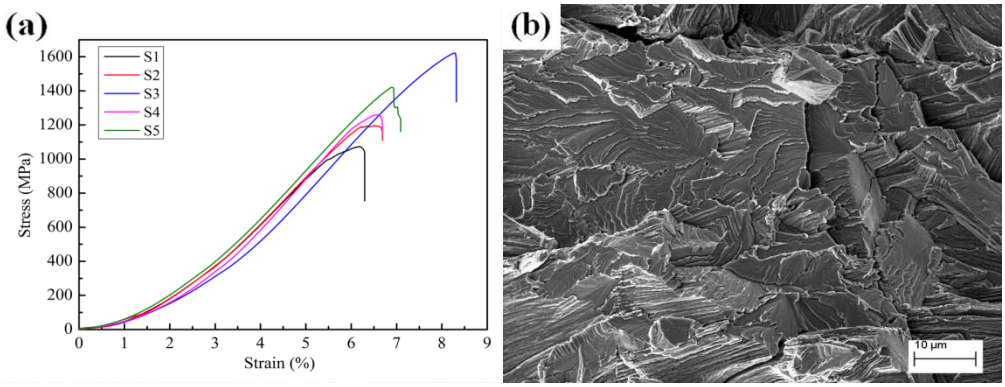

Fig. 6 Compressive properties of the SLM-processed HEA samples.

4. Conclusion

In this study, equiatomic AlCoCuFeNi high-entropy alloy is successfully fabricated via selective laser melting. The laser energy density involved in laser power and scan speed is demonstrated to influence the densification behavior. The HEA part with near full density of >99% can be obtained when the input energy was higher than 102.5 J/mm^3. It shows the SLM-processed HEA parts mainly consist of simple BCC phase and relative high hardness because of solid solution strengthening. Moreover, it was found that microhardness enhanced as the applied laser energy density increased. The optimally produced HEA part with almost-full density exhibited the highest microhardness value up to 541.17 $HV_{0.2}$ and compressive strength of 1621.1 MPa. These optimized parameters were applied for the production of bulk specimens and dodecahedron unit cells as

shown in Fig. 7. The study underpin that SLM is feasible and advantageous to produce high-entropy alloy with high density and good mechanical properties.

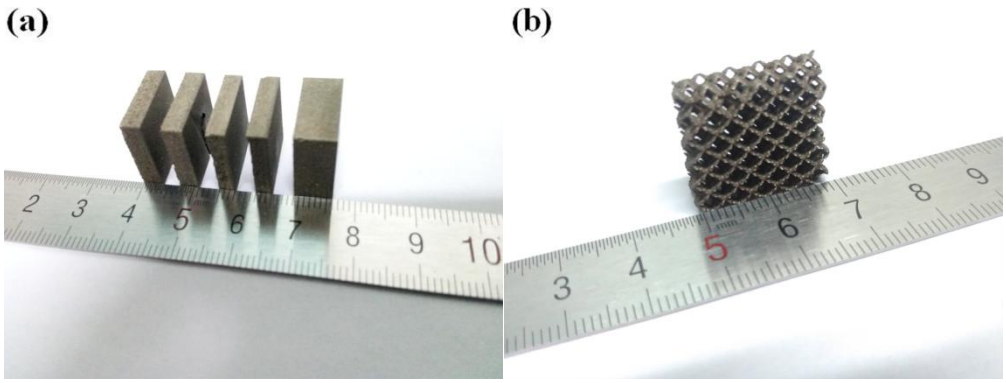

Fig. 7 Photograph of SLM-processed HEA samples with bulk-form and 3D-dodecahedron structures.

Acknowledgements

The work is funded by the National Natural Science Foundation of China (Grant No. 51271034) and the Fundamental Research Funds for the Central Universities (Grant No. FRF-BR-16-023A).

Literature

[1] J.W. Yeh, S.K. Chen, S.J. Lin, J.Y. Gan, T.S. Chin, T.T. Shun, C.H. Tsau, S.Y. Chang, Nanostructured high-entropy alloys with multiple principal elements: novel alloy design concepts and outcomes, Advanced Engineering Materials. 6 (2004) 299–303.

[2] Bin Liu, Jingshi Wang, Yong Liu, Qihong Fang, Yuan Wu, Shiqi Chen, C.T. Liu, Microstructure and mechanical properties of equimolar FeCoCrNi high entropy alloy prepared via powder extrusion, Intermetallics. 75 (2016) 25–30.

[3] Yuan Yu, Jun Wang, Jinshan Li, Hongchao Kou, Weimin Liu, Characterization of BCC phases in $AlCoCrFeNiTi_x$ high entropy alloys, Materials Letters. 138 (2015) 78–80.

[4] Xiaotao Liu, Wenbin Lei, Lijuan Ma, Jing Liu, Jinling Liu, Jianzhong Cui, On the microstructures, phase assemblages and properties of $Al_{0.5}CoCrCuFeNiSi_x$ high-entropy alloys, Journal of Alloys and Compounds. 630 (2015) 151–157.

[5] Chin-You Hsu, Chien-Chang Juan, Woei-Ren Wang, Tsing-Shien Sheu, Jien-Wei Yeh, Swe-Kai Chen, On the superior hot hardness and softening resistance of $AlCoCr_xFeMo_{0.5}Ni$ high-entropy alloys, Materials Science and Engineering A. 528 (2011) 3581–3588.

[6] Ming-Hao Chuang, Ming-Hung Tsai, Woei-Ren Wang, Su-Jien Lin, Jien-Wei Yeh, Microstructure and wear behavior of $Al_xCo_{1.5}CrFeNi_{1.5}Ti_y$ high-entropy alloys, Acta Materialia. 59 (2011) 6308–6317.

[7] Xing Wu Qiu, Yun Peng Zhang, Li He, Chun ge Liu, Microstructure and corrosion resistance of AlCrFeCuCo high entropy alloy, Journal of Alloys and Compounds. 549 (2013) 195–199.

[8] Woei-Ren Wang, Wei-Lin Wang, Jien-Wei Yeh, Phases, microstructure and mechanical properties of $Al_xCoCrFeNi$ high-entropy alloys at elevated temperatures, Journal of Alloys and Compounds. 589 (2014) 143–152.

[9] Yong Dong, Kaiyao Zhou, Yiping Lu, Xiaoxia Gao, Tongmin Wang, Tingju Li, Effect of vanadium addition on the microstructure and properties of AlCoCrFeNi high entropy alloy, Materials and Design. 57 (2014) 67–72.

[10] Tengfei Yang, Songqin Xia, Shi Liu, Chenxu Wang, Shaoshuai Liu, Yong Zhang, Jianming Xue, Sha Yan, Yugang Wang, Effects of AL addition on microstructure and mechanical properties of $Al_xCoCrFeNi$ High-entropy alloy, Materials Science & Engineering A. 648 (2015) 15–22.

[11] A. Popovich, V. Sufiiarov, I. Polozov, E. Borisov, D. Masaylo, A. Orlov, Microstructure and mechanical properties of additive manufactured copper alloy, Materials Letters. 179 (2016) 38–41.
[12] Hu Zhang, Haihong Zhu, Ting Qi, Zhiheng Hu, Xiaoyan Zeng, Selective laser melting of high strength Al–Cu–Mg alloys: Processing, microstructure and mechanical properties, Materials Science & Engineering A. 656 (2016) 47–54.
[13] Zhongji Sun, Xipeng Tan, Shu Beng Tor, Wai Yee Yeong, Selective laser melting of stainless steel 316L with low porosity and high build rates, Materials and Design. 104 (2016) 197–204.
[14] V. Cain, L. Thijs, J. Van Humbeeck, B. Van Hooreweder, R. Knutsen, Crack propagation and fracture toughness of Ti6Al4V alloy produced by selective laser melting, Additive Manufacturing. 5 (2015) 68–76.
[15] J. Sander, J. Hufenbach, L. Giebeler, M. Bleckmann, J. Eckert, U. Kühn, Microstructure, mechanical behavior, and wear properties of FeCrMoVC steel prepared by selective laser melting and casting, Scripta Materialia. 126 (2017) 41–44.
[16] M. Pröbstle, S. Neumeier, J. Hopfenmüller, L.P. Freund, T. Niendorf, D. Schwarze, M. Göken, Superior creep strength of a nickel-based superalloy produced by selective laser melting, Materials Science & Engineering A. 674 (2016) 299–307.
[17] I. Kunce, M. Polanski, K. Karczewski, T. Plocinski, K.J. Kurzydlowski, Microstructural characterisation of high-entropy alloy AlCoCrFeNi fabricated by laser engineered net shaping, Journal of Alloys and Compounds. 648 (2015) 751–758.
[18] Jithin Joseph, Tom Jarvis, Xinhua Wu, Nicole Stanford, Peter Hodgson, Daniel Mark Fabijanic, Comparative study of the microstructures and mechanical properties of direct laser fabricated and arc-melted $Al_xCoCrFeNi$ high entropy alloys, Materials Science & Engineering A. 633 (2015) 184–193.
[19] Hiroshi Shiratori, Tadashi Fujieda, Kenta Yamanaka, Yuichiro Koizumi, Kosuke Kuwabara, Takahiko Kato, Akihiko Chiba, Relationship between the microstructure and mechanical properties of an equiatomic AlCoCrFeNi high-entropy alloy fabricated by selective electron beam melting, Materials Science & Engineering A. 656 (2016) 39–46.
[20] Yevgeni Brif, Meurig Thomas, Iain Todd, The use of high-entropy alloys in additive manufacturing, Scripta Materialia. 99 (2015) 93–96.
[21] Heng Rao, Stephanie Giet, Kun Yang, Xinhua Wu, Chris H.J. Davies, The influence of processing parameters on aluminium alloy A357 manufactured by Selective Laser Melting, Materials and Design. 109 (2016) 334–346.
[22] Y.X. Zhuang, W.J. Liu, Z.Y. Chen, H.D. Xue, J.C. H, Effect of elemental interaction on microstructure and mechanical properties of FeCoNiCuAl alloys, Materials Science & Engineering A. 556 (2012) 395–399.